Mon. Not. R. Astron. Soc. **382,** 1225–1232 (2007) doi:10.1111/j.1365-2966.2007.12440.x

Constraining warm dark matter using QSO gravitational lensing

Marco Miranda[1]★ and Andrea V. Macciò[2]★

[1]*Institute for Theoretical Physics, University of Zürich, Winterthurerstrasse 190, CH-8057 Zürich, Switzerland*
[2]*Max-Planck-Institute for Astronomy, Königstuhl 17, D-69117 Heidelberg, Germany*

Accepted 2007 September 10. Received 2007 September 6; in original form 2007 June 6

ABSTRACT

Warm dark matter (WDM) has been invoked to resolve apparent conflicts of cold dark matter (CDM) models with observations on subgalactic scales. In this work, we provide a new and independent lower limit for the WDM particle mass (e.g. sterile neutrino) through the analysis of image fluxes in gravitationally lensed quasi-stellar objects (QSOs).

Starting from a theoretical unperturbed cusp configuration, we analyse the effects of intergalactic haloes in modifying the fluxes of QSO multiple images, giving rise to the so-called anomalous flux ratio. We found that the global effect of such haloes strongly depends on their mass/abundance ratio and it is maximized for haloes in the mass range 10^6–$10^8\,\mathrm{M}_\odot$.

This result opens up a new possibility to constrain CDM predictions on small scales and test different warm candidates, since free streaming of WDM particles can considerably dampen the matter power spectrum in this mass range. As a consequence, while a (Λ)CDM model is able to produce flux anomalies at a level similar to those observed, a WDM model, with an insufficiently massive particle, fails to reproduce the observational evidences.

Our analysis suggests a lower limit of a few keV ($m_\nu \sim 10$) for the mass of WDM candidates in the form of a sterile neutrino. This result makes sterile neutrino WDM less attractive as an alternative to CDM, in good agreement with previous findings from Lyman α forest and cosmic microwave background analysis.

Key words: gravitational lensing – galaxies: haloes – cosmology: theory – dark matter.

1 INTRODUCTION

The cold dark matter (CDM) model has been successful in explaining a large variety of observational results such as the large-scale structure of the Universe and fluctuations of the cosmic microwave background (CMB; Spergel et al. 2003, 2007). However, the CDM model faces some apparent problems on small scales: namely the overprediction of galactic satellites, the cuspiness and high density of galactic cores and the large number of galaxies filling voids (Klypin et al. 1999; Moore et al. 1999; Avila-Reese et al. 2001; Bode, Ostriker & Turok 2001; Peebles 2001, and references therein). These problems may well have complex astrophysical solutions. For instance, the excess of galactic satellites can be alleviated by feedback processes such as heating and supernova winds that can inhibit the star formation in low-mass haloes (Bullock, Kravtsov & Weinberg 2000).

Another natural cosmological solution to these problems is to replace CDM with a warm species, warm dark matter (ΛWDM; see Bode et al. 2001, and references therein). The warm component acts to reduce the small-scale power, resulting in fewer galactic subhaloes and lower central halo densities.

One of the most promising WDM candidates is a sterile (right-handed) neutrino with a mass in the keV range; such a particle may occur naturally within extensions to the standard model of particle physics (Dodelson & Widrow 1994; Dolgov & Hansen 2002; Asaka, Blanchet & Shaposhnikov 2005; Viel et al. 2005). A sterile neutrino is non-thermal in extensions of the minimal standard model, with a lifetime longer than the age of the universe.

A strong constraint on the mass of WDM candidates comes from Lyman α forest observations (neutral hydrogen absorption in the spectra of distant quasars), since they are a powerful tool for constraining the matter power spectrum over a large range of redshifts down to small scales. Recent analysis of Sloan Digital Sky Survey (SDSS) quasar spectra combined with CMB and galaxy clustering data has set a lower limit on the mass of the sterile neutrino around $m_\nu \approx 10$–13 keV (Seljak et al. 2006; Viel et al. 2006). In this paper, we use a completely different approach to put independent constraints on m_ν, using QSO gravitational lensing and the so-called anomalous flux ratio.

Standard lens models, although they reproduce in general the relative positions of the images quite accurately, often have difficulties explaining the relative fluxes of multiply-imaged sources (Mao & Schneider 1998; Metcalf & Madau 2001; Dalal & Kochanek 2002; Metcalf & Zhao 2002), giving rise to the so-called anomalous flux ratio problem.

★E-mail: solar@physik.unizh.ch (MM); maccio@mpia.de (AVM)

Several possible explanations have been considered in the literature, the most plausible being that the lensing potential of real galaxies is not fully described by the simple lens models used to compute lens characteristics. The most often invoked solution is to consider additional small-scale perturbations (i.e. dark matter haloes), which if located near a photon's light path can modify the overall lens potential (e.g. Raychaudhury, Saha & Williams 2003; Saha, Williams & Ferreras 2007) and significantly alter the observed flux ratio between different images, in particular in the cusp or fold configuration (Metcalf & Madau 2001; Chiba 2002; Chen, Kravtsov & Keeton 2003; Metcalf 2005a,b; Dobler & Keeton 2006). Those perturbers can be roughly divided in two categories: haloes that are inside the primary lens, usually referred as subhaloes, and haloes that are along the line of sight (LOS), in between the source and the observer. This first category of haloes has been extensively studied in the past years both through analytic calculation (Metcalf & Madau 2001; Dalal & Kochanek 2002; Metcalf & Zhao 2002; Keeton 2003) and using numerical simulations (Bradač et al. 2004; Amara et al. 2006; Macciò et al. 2006). The latter two studies have came to the conclusion that the impact of subhaloes on lensing in the mass range 10^7–$10^{10}\,h^{-1}\,\mathrm{M}_\odot$ is very small. Even considering the impact of less massive subhaloes, usually not resolved in *N*-body/hydro-simulations, does not help in reproducing the observed number of anomalous flux ratios (Macciò & Miranda 2006).

The effect of the second category of haloes, those along the LOS, is still somewhat controversial (Chen et al. 2003; Metcalf 2005a,b). In particular, Metcalf (2005a,b) found that dark matter haloes with masses around 10^6–$10^8\,\mathrm{M}_\odot$ can produce anomalies in the flux ratios at a level similar to those that are observed. The presence of a WDM particle even with a mass around 10 keV will strongly reduce the number density of such small mass haloes, giving a different signature to the image fluxes. As a consequence, the observed anomalous flux ratios can be used to constrain the abundance of small haloes along the LOS and therefore to put an independent constraint on the mass of the sterile neutrino as a possible WDM candidate.

In this paper, we analyse in detail the effect of subhaloes along the LOS on an unperturbed cusp configuration in a ΛCDM model and in ΛWDM models with different values of m_ν. We found that WDM models with $m_\nu < 10$ keV fail to reproduce the observed anomalies in the lensed QSO flux ratios. Our results provide a new and independent constraint on the mass of sterile neutrino, and they are in good agreement with previous constraints coming from Lyman α forest and CMB analysis.

The format of this paper is as follows. In Section 2, we compute the expected halo abundance in different models; in Section 3 we briefly review the lensing formalism we adopt. Section 4 is devoted to the description of our lensing simulations. In Section 5, we present the numerical results, matching them with observations. We conclude with a short summary and discussion of our results in Section 6.

2 INTERGALACTIC HALO MASS FUNCTION

The main goal of this work is to study the effect of dark matter haloes along the LOS on fluxes of QSO multiple images. In order to achieve it, we first computed the number density of those haloes in the light cone between the source plane and the observer.

For this purpose, we used the Sheth and Tormen mass function (ST; Sheth & Tormen 2002), taking into account its evolution with redshift. We adopted a *Wilkinson Microwave Anisotropy Probe WMAP1*-like cosmology (Spergel et al. 2003) with the following values for dark energy and dark matter density, normalization and slope of the matter power spectrum: $\Omega_\Lambda = 0.74, \Omega_\mathrm{m} = 0.26, \sigma_8 = 0.9$ and $n = 1$.

The transfer function for the CDM model has been generated using the public code CMBFAST (Seljak & Zaldarriaga 1996). To compute the transfer function for WDM models, we used the fitting formula suggested by Bode et al. (2001):

$$T^2(k) = \frac{P^\mathrm{WDM}}{P^\mathrm{CDM}} = [1 + (\alpha k)^{2\nu}]^{-10/\nu}, \quad (1)$$

where α, the scale of the break, is a function of the WDM parameters, while the index ν is fixed. Viel et al. (2005, see also Hansen et al. 2002), using a Boltzmann code simulation, found that $\nu = 1.12$ is the best fit for $k < 5\,h\,\mathrm{Mpc}^{-1}$, and they obtained the following expression for α:

$$\alpha = 0.049 \left(\frac{m_x}{1\,\mathrm{keV}}\right)^{-1.11} \left(\frac{\Omega_\nu}{0.25}\right)^{0.11} \left(\frac{h}{0.7}\right)^{1.22} h^{-1}\,\mathrm{Mpc}. \quad (2)$$

This expression applies only to the case of thermal relics. In order to apply it to a sterile neutrino, we take advantage of the one-to-one correspondence between the masses of thermal WDM particles (m_x) and sterile neutrinos (m_ν) for which the effect on the matter distribution and thus the transfer function for both models is identical (Colombi, Dodelson & Widrow 1996). We used the m_x– m_ν relation given by Viel et al. (2005), that reads

$$m_{\nu,\mathrm{sterile}} = 4.43 \left(\frac{m_{x,\mathrm{thermal}}}{1\,\mathrm{keV}}\right)^{4/3} \left(\frac{0.25}{\Omega_\nu}\right)^{1/3} \left(\frac{0.7}{h}\right)^{2/3} \mathrm{keV}. \quad (3)$$

We used the expression given in equation (2) for the damping of the power spectrum for simplicity and generality. More accurate expressions for the damping for concrete models of sterile neutrinos exist (Abazajian 2006; Asaka, Shaposhnikov & Laine 2007) and show that the damping depends on the detailed physics of the early universe in a rather non-trivial way. Naturally, the results of this paper can be repeated using other expressions for the damping.

The main effect of WDM is to dampen the power spectrum of fluctuation on small scales, reducing the number of haloes at low masses (Bode et al. 2001; Barkana, Haiman & Ostriker 2001; Paduroiu et al., in preparation). Fig. 1 shows the ration between halo number density in WDM and CDM models as a function of the WDM mass m_ν.

Typically, lensed QSOs are located at a redshift of around 3. This implies that we also need to take into account the redshift evolution

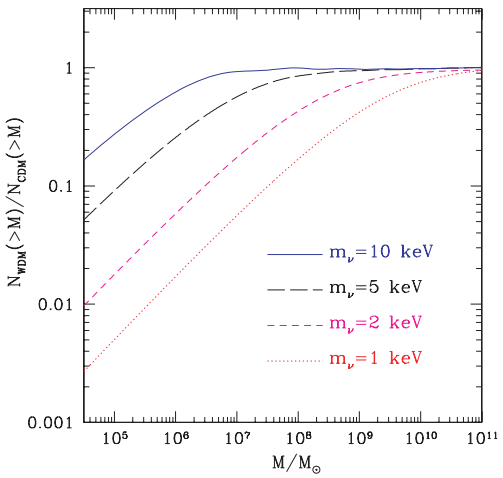

Figure 1. Effects of WDM particles on the dark matter halo mass function at redshift zero.

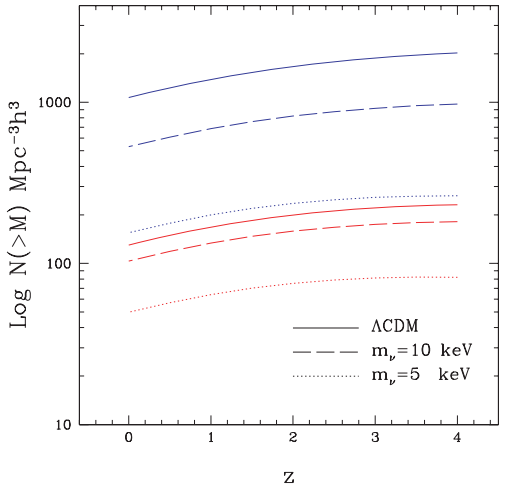

Figure 2. Evolution with redshift of the number of haloes above a fixed mass threshold in different models. The uppermost solid (blue) line is for $M > 10^6\,h^{-1}\,\mathrm{M}_\odot$ in the ΛCDM model; the dashed and the dotted lines are for the same mass threshold but for a WDM mass of $m_\nu = 10,\,5\,\mathrm{keV}$, respectively. The second set of (red) lines refers to a mass threshold of $M > 10^7\,h^{-1}\,\mathrm{M}_\odot$.

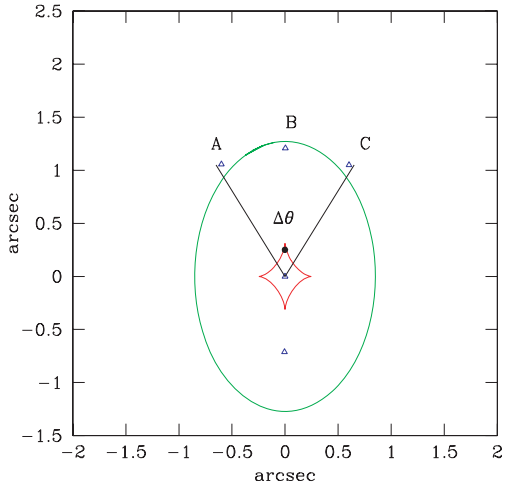

Figure 3. Unperturbed cusp configuration: $R_{\rm cusp} = 0.09$. The source and image positions are marked by a solid circle and open triangles, respectively. The opening angle is also shown.

of the mass function in different models. Fig. 2 shows the number of haloes more massive than $10^6\,h^{-1}\,\mathrm{M}_\odot$ (upper solid curve) and $10^7\,h^{-1}\,\mathrm{M}_\odot$ (lower solid curve) per Mpc cube at different redshifts. It is interesting to note that on such small mass scales, the halo number density tends to increase towards high redshift. We found that the evolution of the mass function, both in CDM and in WDM models, can be well represented by the following fitting formula:

$$\log N(>M, z) = N_0 + 0.11 z^{0.7}, \tag{4}$$

where N_0 is the logarithm of the halo number density at redshift zero [$N_0 = \log N(>M, z = 0)$]. The use of this fitting formula has the advantage of speeding up the calculation of the number of haloes in each lensing plane (see Section 4).

To conclude this section, we want to emphasize that our particular choice of cosmological parameters does not influence the results we will present in the next section. For instance, on the mass scales we are interested in ($M < 10^{10}\,h^{-1}\,\mathrm{M}_\odot$) changing σ_8 from 0.9 to 0.7 would increase the number of haloes only by a few per cent.

3 LENSING FORMALISM

We briefly recall the general expressions for gravitational lensing and refer, for example, to Schneider, Ehlers & Falco (1992) (hereafter SEF) for more details. The lens equation is defined as

$$\boldsymbol{\theta} = \boldsymbol{\beta} + \boldsymbol{\alpha}(\boldsymbol{\theta}), \tag{5}$$

where $\boldsymbol{\beta}(\boldsymbol{\theta})$ is the source position and $\boldsymbol{\theta}$ the image position. $\boldsymbol{\alpha}(\boldsymbol{\theta})$ is the deflection angle, which depends on $\kappa(\boldsymbol{\theta})$ the dimensionless surface mass density (or convergence) in units of the critical surface mass density $\Sigma_{\rm crit}$, defined as

$$\Sigma_{\rm crit} = \frac{c^2}{4\pi G}\frac{D_S}{D_L D_{LS}}, \tag{6}$$

where D_S, D_L, D_{LS} are the angular diameter distances between observer and source, observer and lens, source and lens, respectively.

3.1 The cusp relation

There are basically three configurations of four-image systems: fold, cusp and cross (Schneider & Weiss 1992). In this paper, we will mainly concentrate on the *cusp* configuration, that corresponds to a source located close to the cusp of the inner caustic curve (see Fig. 3). The behaviour of gravitational lens mapping near a cusp was first studied by Blandford & Narayan (1986), Schneider & Weiss (1992) and Zakharov (1995), who investigated the magnification properties of cusp images and concluded that the sum of the signed magnification factors of the three merging images approaches zero as the source moves towards the cusp. In other words,

$$R_{\rm cusp} = \frac{\mu_A + \mu_B + \mu_C}{|\mu_A| + |\mu_B| + |\mu_C|} \to 0, \quad \text{for} \quad \mu_{\rm tot} \to \infty, \tag{7}$$

where $\mu_{\rm tot}$ is the unsigned sum of magnifications of all four images, and A, B & C are the triplet of images forming the smallest opening angle (see Fig. 3). By opening angle, we mean the angle measured from the galaxy centre and spanned by two images of equal parity. The third image lies inside such an angle. This is an asymptotic relation and holds when the source approaches the cusp from inside the inner caustic 'astroid'. This can be shown by expanding the lensing map to third order in the angular separation from a cusp (Schneider & Weiss 1992). Structure on scales smaller than the image separation will cause $R_{\rm cusp}$ to differ from zero fairly independently of the form of the rest of the lens. Note that by definition of $R_{\rm cusp}$ used here, it can be either positive or negative. A perturber is more likely to reduce the absolute magnification for negative magnification images (Metcalf & Madau 2001; Schechter & Wambsganss 2002; Keeton 2003) and to increase it for positive parity images. As a result, the probability distribution of $R_{\rm cusp}$ will be skewed toward positive values.

3.2 The unperturbed lens

We used the GRAVLENS code (Keeton 2001)[1] to create a lens configuration for which the cusp relation is roughly satisfied (see Fig. 3).

[1] The software is available via the web site http://cfa-www.harvard.edu/castles

The main, smooth, lens has been modelled as a singular isothermal ellipsoid (SIE) (Kormann, Schneider & Bartelmann 1994) to take advantage of its simplicity. This model has been widely used in lens modelling and successfully reproduces many lens systems (e.g. Keeton, Kochanek & Falco 1998; Chiba 2002; Treu & Koopmans 2002). The ellipsoidal primary lens has a mass equal to $5 \times 10^{11}\,\mathrm{M}_{\odot}$, is oriented with the major axis along the y-axis in the lens plane and has an ellipticity of 0.33. The redshift of the lens has been fixed to $z_l = 0.3$ in agreement with typical observed ones (i.e. Tonry 1998). The cusp relation, defined by equation (7), for this smooth lens gives $R_{\mathrm{cusp}} = 0.09$, and this is one of the configurations previously studied in Macciò & Miranda (2006, namely Config2). We tested that our results do not depend on this particular choice for the unperturbed configuration and do apply to any cusp configuration.

4 SUBHALOES ALONG THE LOS: IDEA AND PROCEDURE

The purpose of this work is to compute the effects of intergalactic haloes, along the LOS, on an unperturbed cusp lensing configuration to extract information on the matter power spectrum on small scales. In this approach, we model our haloes as singular isothermal spheres (SIS). A SIS, with density profile $\rho \propto r^{-2}$, is a simple model that is often used in lensing because its simplicity permits detailed analytic treatment (e.g. Finch et al. 2002). The model has been used to represent mass clumps for studies of substructure lensing, after taking into account tidal stripping by the parent halo (Metcalf & Madau 2001; Dalal & Kochanek 2002). Again, the simplicity of the SIS makes it attractive for theoretical studies: a tool that not only reveals, but also elucidates, some interesting general principles. For the $10^6\,\mathrm{M}_{\odot}$ haloes relevant for this work, the SIS profile does not differ dramatically from the NFW (Navarro, Frenk & White 1996) profile inferred from cosmological N-body simulations (Keeton 2003). Besides, the SIS model yields *conservative* results. Since a NFW halo is centrally less centrally concentrated than a SIS halo, it is less efficient as a lens and therefore would have to be more massive in order to produce a given magnification perturbation. Macciò & Miranda (2006) have shown that a SIS model will induce lensing effects marginally stronger than those caused by a NFW profile with concentration parameter $c \sim 55$ corresponding to a mass around $10^6\,\mathrm{M}_{\odot}$. Haloes in a WDM model are expected to be less concentrated due to the top-down structure formation scenario (Eke, Navarro & Steinmetz 2001; Paduroiu et al., in preparation). In this case, the SIS approximation can possibly overestimate the total effect of WDM perturbers, making our lower bound to the WDM particle mass even stronger.

A SIS halo model is completely characterized by its Einstein radius:

$$\theta_{\mathrm{E}} = \frac{4\pi\sigma^2}{c^2}\frac{D_{LS}}{D_S}, \tag{8}$$

where σ is the halo velocity dispersion, and D_S, D_{LS} are the angular diameter distances introduced in Section 3. We adopt a source redshift $z_{\mathrm{s}} = 2$. We filled the portion of Universe along the LOS with cubes, then the subhaloes inside each cube were projected on to the middle plane (see Fig. 4). We used a total of 100 different lens planes roughly equally distributed in space between the source and the observer. This results in $N_1 = 85$ planes behind the main lens and $N_2 = 15$ planes in front of it. The size of the cubes was defined as follows.

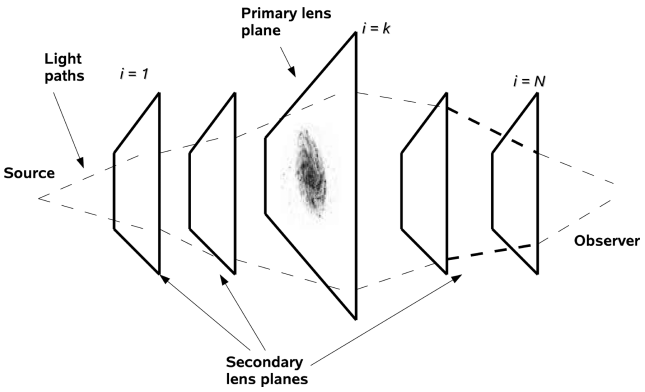

Figure 4. A schematic diagram of the type of lensing system being considered. There is one primary lens responsible for the multiple images of the source. In addition, there are many secondary lenses (most not shown). The unperturbed light paths are deflected only by the primary lens and with an appropriate model for the primary lens will meet on the source plane. If the deflections from secondary lens planes are taken into account without changing the primary lens model, the light will follow the perturbed light paths (dashed curves). This diagram is not to scale in any respect.

Two close planes were separated by $\Delta z_1 = (z_{\mathrm{max}} - z_l)/N_1$ if situated behind the main lensing galaxy, and by $\Delta z_2 = (z_l - z_{\mathrm{min}})/N_2$ for planes in front if it, where $z_{\mathrm{min}} = 0.01$ and $z_{\mathrm{max}} = z_{\mathrm{s}} - 0.1$.

The size of a comoving volume inside a solid angle $d\Omega$ and a redshift interval d z is given by (Hogg 1999)

$$\mathrm{d}V_{\mathrm{C}} = D_{\mathrm{H}}\,\frac{(1+z)^2\,D_{\mathrm{A}}^2}{E(z)}\,\mathrm{d}\Omega\,\mathrm{d}z \tag{9}$$

where D_{A} is the angular diameter distance at redshift z and $E(z)$ is defined as

$$E(z) \equiv \sqrt{\Omega_{\mathrm{M}}\,(1+z)^3 + \Omega_{\mathrm{k}}\,(1+z)^2 + \Omega_{\Lambda}} \tag{10}$$

with $\Omega_{\mathrm{M}}, \Omega_{\mathrm{k}}$ and Ω_{Λ} the density parameters of matter (cold and warm), curvature and cosmological constant, respectively.

We populated each cube with dark matter haloes, whose total number and mass distribution were chosen according to the ST mass function at the appropriate redshift (see Section 2). Halo positions and redshifts (within $\Delta z_{1,2}$) were randomly assigned. Within a solid angle $d\Omega$ of 3×3 arcsec^2, the total number of haloes with mass larger than $10^6\,\mathrm{M}_{\odot}$ comes to 512 for the ΛCDM model adopted in this paper. This number drops in a consistent way in a WDM scenario, depending on m_v. For a WDM particles mass of 10 keV, we obtain 238 haloes along the LOS within the same dΩ, and even fewer (156, 135) for a less massive choice for m_v (7.5, 5 keV; see Fig. 1).

Since we are interested in flux anomalies, we consider only cases in which we do not have image splitting due to the extra haloes along the LOS. Therefore, we do not allow any of those haloes to be closer than twice its Einstein radius (θ_{E}) from any images in order to prevent image splitting (see SEF and references therein). On average, only few haloes (three, for ΛCDM) fail in satisfying this criterion and we tested their removal/inclusion does not affect the final R distribution in any way. Let η denote the two-dimensional position of the unperturbed image with respect to the perturber on the I plane, measured with respect to the intersection point of the optical axis with the I plane and ξ the light ray impact parameter on the I' plane. In the absence of image splitting, a SIS perturber will affect the position of each image according the following:

$$\eta = \xi\,\frac{D_I}{D_I'} - \alpha(\xi) D_{I'I}. \tag{11}$$

Introducing the angular coordinates $\eta = D_I\theta_I$ and $\xi = D'_I\theta'_I$, and given that $\alpha(\xi) = \theta_E$ for a SIS, the equation for the flux becomes

$$\mu = \frac{\theta'_I}{\theta'_I - \theta_E}, \tag{12}$$

where the quantities with subindex I refer to the (unperturbed) image position with respect to the perturber and so D_I, $D_{I'}$, $D_{I'I}$ are the distances between observer and the I plane, observer and I' plane, I plane and I' plane, respectively. On each single lens plane, the total effect on the image magnification factor μ is obtained by summing up contributions by each perturber. In principle, one should sum the magnification tensors first and then take the determinant. The two methods (scalar or matrix sum) do not lead to the same result because $\det(A + B) \neq \det(A) + \det(B)$. In the case of scalar sum and two SIS perturbers with Einstein radii $\theta_{E,1}$ and $\theta_{E,2}$, the total magnification depends on the order in which the two lenses act on the source: $\mu_{1,2}$ is different from $\mu_{2,1}$. The error introduced by a direct sum is of the order of the ratio between the $\mu_{1,2}$ and $\mu_{2,1}$. This quantity can be directly computed from equations (11) and (12) and it is always $< \max(\theta_{E,1}, \theta_{E,2})/\beta$. In our case, due to the low mass of our perturbers, the ratio $\theta_I/\theta_{E,i}$ is of the order of 200–800, which gives an error less than 1 per cent for the total μ. There is still a small chance to have a substructure located at a place where $\theta_I \approx \theta_{E,i}$. We looked for this possibility and it happened only eight times over 100 000 substructure position realizations, giving a negligible effect on the final averaged value of R_{cusp}.

Generally, a matter clump will change the positions of the images slightly, so if a lens model is chosen to fit the observed image positions perfectly, it will not do it anymore after the perturber is added. To produce a perfectly consistent lens model, one would have to adjust the main lens model for each realization of the intergalactic haloes. This is very computationally expensive and not necessary in practice. The shifts in positions are generally small when the masses of the secondary lenses are small ($\approx$0.1 arcsec for $M \approx 10^8\,M_\odot$; Metcalf 2005a) and, in addition, since the host lens model is degenerate it is ambiguous how it should be adjusted to correct for the shift. The goal here is to reproduce all the significant characteristics of the effects induced by the observed lens (image configuration, fluxes) so that one can determine whether lenses, that look like the observed ones and have the observed ratio anomalies, are common in CDM/WDM models. For the source, we adopt the point-like approximation. The importance of considering the source size lies mainly in the capability to disentangle different subhaloes mass limits (Chiba et al. 2005; Dobler & Keeton 2006). As remarked by Chang & Refsdal (1979) and many authors afterwards (see Metcalf 2005a, and references therein), the projected size (on the lens plane) of the emitting regions of QSOs is expected to be different and this can be used to remove, eventually, lens model degeneracy and improve the sensitivity to substructure properties. In our cases, the size of the radio emitting region, when projected on the lens plane, is expected to be affected by structures with masses larger than $10^5\,M_\odot$ (Metcalf 2005a,b).

In a single realization of our perturbed lens configuration, the light coming from the source is deflected by $\approx$500 haloes (plus the main lens) before reaching the observer. Each one of the three images forming the cusp configuration is shifted and amplified, giving as a result a modified R_{cusp} value, different from the original (unperturbed) one of $R_{cusp} = 0.09$. Sometimes, when a massive halo ($M > 10^8\,M_\odot$) happens to be close to one of the images, this image can be strongly deflected, resulting in a breaking of the cusp configuration. In the statistical studies presented here, these cases are simply excluded from the final sample. In total, we performed 2000 realizations (with different random seeds for generating masses and positions of perturbers) of each model (CDM/WDM), obtaining 2000 different final lensing configurations. For some of these final configurations (with high R_{cusp} values), we try to fit image positions and magnification factors with the GRAVLENS code, using a smooth lens model. While it is relatively simple to reproduce the image geometrical properties, it is never possible to get the right flux ratios, with such a simple model.

5 RESULTS

The first part of this section is devoted to presenting the effects of haloes along the LOS on the cusp relation in a standard (Λ)CDM scenario. The plots show the probability distribution for the cusp relation value, considering 2000 different realizations of the same model. Those realizations share the same total number of perturbers, but differ in their masses (randomly drawn from a ST distribution), positions (randomly assigned within the lens plane) and redshifts (randomly chosen within $\Delta z_{1,2}$).

The cusp relation defined by equation (7) holds when the source is close to the cusp. As soon as the source moves away from the cusp, deviations from $R_{cusp} = 0$ are observed, even for the smooth lens model. On the other hand, the closer the source is to the cusp, the smaller is the angle spanned from the three images. Therefore, in order to take into account the position of the source in evaluating the cusp relation, it is better to define the anomalous flux ratio as

$$R = \frac{2\pi}{\Delta\theta} R_{cusp}, \tag{13}$$

where $\Delta\theta$ is the opening angle spanned by the two images with positive parity defined from the centre of the galaxy. With this new definition of the cusp relation, a set of three images is said to violate the cusp relation if $R > 1$. This makes the comparison between simulations and observations much more straightforward. For this comparison, we used the same data presented in Macciò et al. (2006). There are five observed cusp caustic lenses systems (summarized in Table 1): B0712+472 (Jackson et al. 1998), B2045+265 (Koopmans et al. 2003), B1422+231 (Patnaik & Narasimha 2001), RXJ1131−1231 (Sluse et al. 2003) and RXJ0911+0551 (Keeton 2003); the first three are observed in the radio band and the last two in optical and IR. Three of them violate the reduced cusp relation (i.e. $R > 2\pi/\Delta\theta$).

Fig. 5 shows the R probability distribution for the three possible categories of perturbers. The dotted (red) line shows the effect of subhaloes inside the primary lens that can be directly tested by current numerical simulations (i.e. with masses $>10^7\,M_\odot$; Macciò et al. 2006). The short-dashed (cyan) line shows the effect of lower mass subclumps (still inside the primary lens) as measured by Macciò & Miranda (2006). The solid (blue) line shows the effect of the haloes along the LOS considered in this work; here, we considered only haloes with $M > 5 \times 10^6\,M_\odot$. As already noted, the first two categories of perturbers fail in reproducing the high value tail that arises

Table 1. The image opening angles and cusp caustic parameters for the observed cusp caustic lenses.

Lens	$\Delta\theta$	R_{cusp}	Obs. band
B0712+472	79.°8	0.26 ± 0.02	Radio
B2045+265	35.°3	0.501 ± 0.035	Radio
B1422+231	74.°9	0.187 ± 0.006	Radio
RXJ1131−1231	69.°0	0.355 ± 0.015	Optical/IR
RXJ0911+0551	69.°6	0.192 ± 0.011	Optical/IR

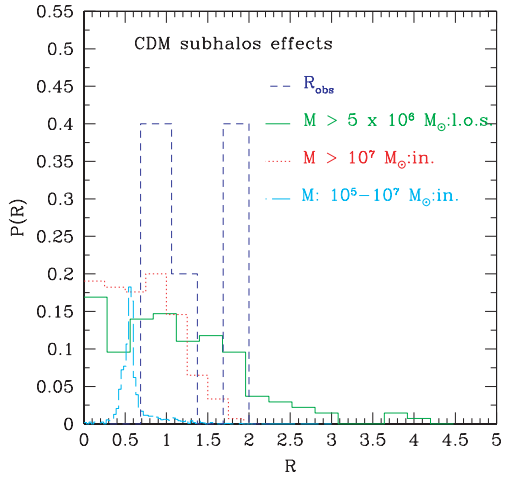

Figure 5. *R* probability distribution for different categories of (sub)haloes within the CDM scenario. The dotted line shows the effect of substructures (with $M > 10^7\,M_\odot$) inside the lens galaxy (Macciò et al. 2006); the long-dashed line is for less massive subhaloes ($M = 10^5$– $10^7\,M_\odot$) still inside the primary lens (Macciò & Miranda 2006). The solid line is for the haloes along the LOS with mass $>5 \times 10^6\,M_\odot$ studied in this work. Observational results are also shown (long dash histogram).

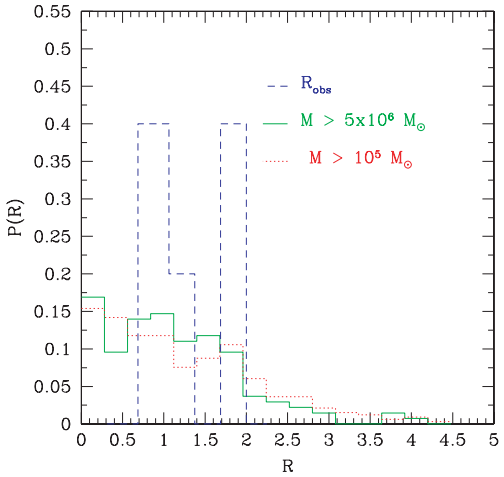

Figure 6. *R* distribution for haloes along the LOS for two choices of their minimum mass: $M > 10^5$ (dot line) and $M > 5 \times 10^6\,M_\odot$ (solid line). The dashed histogram shows the observational data.

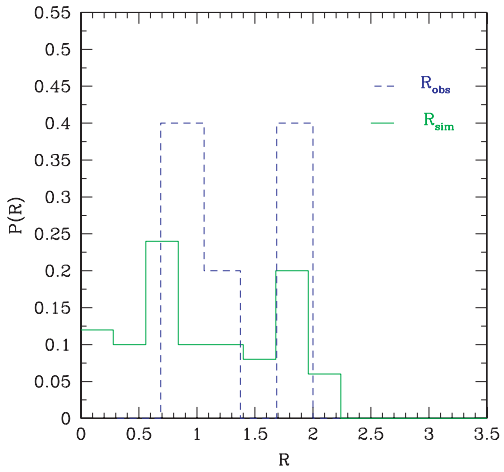

Figure 7. *R* probability distribution for CDM considering a lower number of realization (≈200) in the averaging process (see text). The dashed histogram shows the observational data.

in the observational data around $R = 2$. On the contrary, the signal coming from haloes along the LOS has a probability distribution which remains almost flat in *R* range 1–2, where two (out of five) of the observed systems lay.

Thanks to this pronounced tail at high *R* value, haloes filling the light cone between the source and the observer can easily account for all the observed cusp systems, providing a solution to the anomalous flux ratio issue. Our results are in fair agreement with those previously obtained by Metcalf (2005b) and seem to confirm that a previous result on the same subject obtained by Chen et al. (2003) did underestimate the effects of intergalactic structure. Chen et al. (2003) used the cross-section (or optical-depth) method to calculate the magnification probability distribution. This method is mainly valid for rare events and this is not the case since, as shown in Section 4, the number of lensing events is of the order of 500. A more detailed and general comparison of the two methods can be found in Metcalf (2005b). In Metcalf (2005b), the author used an approach similar to that of ours, making a direct lensing simulation in order to compute the effects of haloes along the LOS, modelling them using a NFW density profile. Although in his work the author analysed each observed configuration separately, finding slightly different individual *R* probabilities for different systems, the similarity of the results is a good proof a posteriori that our assumptions of SIS parametrization for perturbers and point-source approximation did not introduce a strong bias in the results.

In the previous analysis, we restricted the mass range to haloes more massive than $M = 5 \times 10^6\,M_\odot$. In Fig. 6, the probability distribution for *R* is shown for two different choices of the minimum halo mass: $M > 5 \times 10^6\,M_\odot$ (solid, blue line) and $M > 10^5\,M_\odot$. In the latter case, the total number of structures is around 5 500 and the lensing simulation code slows down considerably. A close comparison of the two histograms clearly shows that considering less massive haloes does not improve the results substantially; so in the following we will only consider haloes with $M > 5 \times 10^6\,M_\odot$.

In some cases, when the averaging process is restricted to a lower number of realizations (∼200) we found that the observational data are reproduced with a high confidence level as shown in Fig. 7.

These results are probably due to effects induced by single massive perturbers close to a particular image: or a positive image is highly magnified or a negative one is demagnified [note that in equation (7) we consider the absolute values for μ_i], providing an anomalous *R*. While with a low number of realizations (∼200) these single events contribute significantly to the global *R*, a higher number of realizations (>10 000) permits all the images to be affected by massive clumps, smoothing the final probability distribution.

The introduction of a WDM particle damps the matter power spectrum on small scales, reducing the number of haloes along the LOS. In Fig. 8, we show the probability distribution of *R* as a function of the mass of the WDM candidate. Changing the WDM particle mass from $m_\nu = 12.5$ to $m_\nu = 7.5$ keV drops the tail at $R = 2$ from a 10 per cent probability to a 1.5 per cent one. For $m_\nu = 5$ keV, we have a $P(R)$ higher than 5 per cent only for $R < 1.3$. In the latter case, only 20 haloes are inside the volume sampled by the three images, and this model tends to leave the value of *R* close to the unperturbed one. A model with a 10 keV sterile neutrino, if compared to a model with $m_\nu = 12.5$ keV, gives a slightly

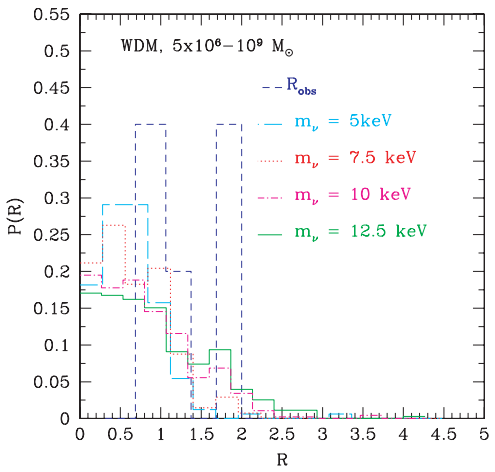

Figure 8. Probability distributions for different warm particle masses: $m_\nu = 5$ keV (long-dashed line), $m_\nu = 7.5$ keV (dot line), $m_\nu = 10$ keV (dash–dotted line) and $m_\nu = 12.5$ keV (solid line). Dashed line shows the probability distribution of observational data.

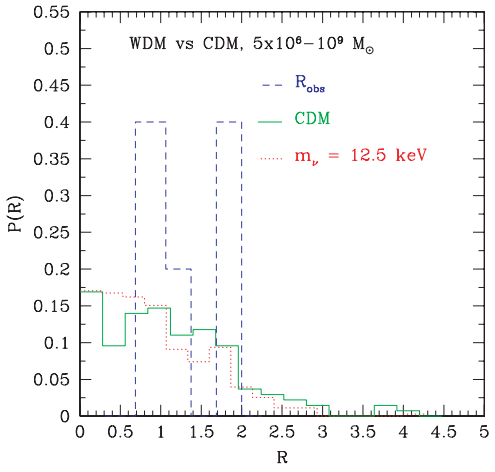

Figure 9. R distribution probability for: observed values (dashed line), CDM haloes more massive than 5×10^6 M$_\odot$ (solid line) and WDM subhaloes with $m_\nu = 12.5$ keV (dotted line).

lower probability (8 versus 10 per cent) to have a configuration with $R = 2$. Due to the limited number of observed cusp systems, it is hard to disentangle those two models, and we think that it is fair to say that $m_\nu = 10$ keV is still in agreement with the data.

Fig. 9 shows the comparison between the observational data, the standard (Λ)CDM model and a WDM model with a sterile neutrino mass of 12.5 keV, which is close to the current limit provided by Lyman α + CMB analysis (Seljak et al. 2006). In this case, in both the warm and the CDM scenario, haloes along the LOS can easily account for the two observed cusp systems with $R \approx 2$, offering a viable solution to the anomalous flux ratio issue. On the contrary, a WDM model with less massive particles (i.e. with a higher free streaming scalelength) fails in reproducing the observational data due to the reduced number density of haloes along the LOS.

6 DISCUSSION AND CONCLUSIONS

Interest in WDM models has been sporadic over the years, although this class of models could help alleviate several problems on small scales that occur with CDM. In order to constrain the WDM scenario, precise measurements of the matter power spectrum on small scales are needed; for this purpose, Lyman α forest and CMB data have been extensively used (Seljak et al. 2006; Viel et al. 2006).

In this paper, we show that image flux ratios in multiple gravitationally lensed QSOs can be modified by haloes along the LOS in the mass range 10^6– 10^7 M$_\odot$; this effect opens a new window to study the matter power spectrum on small scales and provides a new and independent method to constrain the mass of WDM candidates m_ν.

The observed anomalous flux ratio in lensed QSOs can be explained by adding small perturbations to the smooth model used to parametrize the main lenses. Those perturbers can be identified with dark matter haloes that happen to be close to the images' light paths. Recent results based on numerical N-body (Amara et al. 2006; Rozo et al. 2006) and hydrodynamical simulations have shown that it is hard to reconcile the observed high number of cusp relation violations with the total number of substructures inside the primary lens predicted by the ΛCDM model. This is true even when the limited mass resolution of numerical simulations is taken into account (Macciò & Miranda 2006).

The hierarchical formation scenario predicts that the universe should be filled by a large number (more than 10^3 per h^{-1} Mpc^3) of dark matter haloes with masses $M \approx 10^6$ M$_\odot$. We employed the Sheth & Tormen mass function to estimate the expected number of haloes in this mass range along the LOS of lensed QSOs. We found that on average there are more than 500 haloes in between the source and the observer, within a light cone with an aperture of 3 arcsec. Using direct lensing simulations and a SIS approximation, we computed the effects of those haloes on an unperturbed cusp configuration. We generated more than 10^4 different realizations of our global (lens + perturbers) lensing system, varying masses, positions and number of haloes.

We found that on a statistical basis (averaging on different realizations), this class of perturbers can modify consistently the fluxes of QSO multiple images at a level comparable to the observed one, in good agreement with previous studies on this subject (Metcalf 2005a,b). In some cases, when the averaging process is restricted to a lower number of realizations (≈200; see Fig. 7) we found that the observational data are reproduced with a high confidence level.

An important result of our study is that the bulk of the signal on QSO fluxes is due to haloes in the mass range 10^6– 10^7 M$_\odot$. Since the number density of such haloes, and therefore their effect on the cusp relation, can be strongly damped by the presence of a WDM candidate, the observed number of anomalous flux ratios can be used to constrain the mass of WDM particles.

Adding an exponential cut-off to the transfer function of WDM models, we computed the number density of small haloes as a function of the mass of the warm particles. We show that if WDM is due to a sterile neutrino, then, in models with $m_\nu < 10$ keV, the number of dark haloes along the LOS is too low to affect in a consistent way the fluxes of lensed QSOs, failing to reproduce the observed abundance of systems with high R values. This lower limit for the mass of the sterile neutrino is in good agreement with results obtained using different methods.

The main limitation of this study is represented by the few observational data that are available in the literature. However, future experiments such as DUNE (Réfrégier et al. 2006), are likely to observe more then 1000 lensed quasars, of which several hundreds should be quadruples due to the magnification bias. It will provide new lensing systems to be analysed and thus more tightly constrain the WDM scenario.

ACKNOWLEDGMENTS

It is a pleasure to thank S. Hansen for enlightening discussion about WDM, P. Saha for useful hints on the lensing simulations and K. Blindert for carefully reading the manuscript. We also thank the referee (HongSheng Zhao) for his useful comments that improved the presentation of our work and M. Bartelmann and D. Sluse for discussions during the preparation of this paper. MM thanks the MPIA Heidelberg for their hospitality while this paper was being completed. All the numerical simulations were performed on the zBox1 supercomputer (www.zbox1.org) at the University of Zürich. MM was partially supported by the Swiss National Science Foundation.

REFERENCES

Abazajian K., 2006, Phys. Rev. D., 73, 063506
Amara A., Metcalf R. B., Cox T. J., Ostriker J. P., 2006, MNRAS, 367, 1367
Asaka T., Blanchet S., Shaposhnikov M., 2005, Phys. Lett. B., 631, 151
Asaka T., Shaposhnikov M., Laine M., 2007, J. High Energy Phys., 1, 91
Avila-Reese V., Colín P., Valenzuela O., D'Onghia E., Firmani C., 2001, ApJ, 559, 516
Barkana R., Haiman Z., Ostriker J. P., 2001, ApJ, 558, 482
Blanford R., Narayan R., 1986, ApJ, 310, 568
Bode P., Ostriker J. P., Turok N., 2001, ApJ, 556, 93
Bradač M., Schneider P., Lombardi M., Steinmetz M., Koopmans L. V. E., Navarro J. F., 2004, A&A, 423, 797
Bullock J. S., Kravtsov A. V., Weinberg D. H., 2000, ApJ, 539, 517
Chang K., Refsdal S., 1979, Nat, 282, 561
Chen J., Kravtsov A. V., Keeton C. R., 2003, ApJ, 592, 24
Chiba M., 2002, ApJ, 565, 71
Chiba M., Minezaki T., Kashikawa N., Kataza H., Inoue K. T., 2005, ApJ, 627, 53
Colombi S., Dodelson S., Widrow L. M., 1996, ApJ, 458, 1
Dalal N., Kochanek C. S., 2002, ApJ, 572, 25
Dobler G., Keeton C. R., 2006, MNRAS, 365, 1243
Dodelson S., Widrow L. M., 1994, Phys. Rev. Lett., 72, 17
Dolgov A. D., Hansen S. H., 2002, Astropart. Phys., 16, 339
Eke V. R., Navarro J. F., Steinmetz M., 2001, ApJ, 554, 114
Finch T. K., Carlivati L. P., Winn J. N., Schechter P. L., 2002, ApJ, 577, 51
Hansen S. H., Lesgourgues J., Pastor S., Silk J., 2002, MNRAS, 333, 544
Hogg D., 1999, preprint (astro-ph/9905116)
Jackson N. et al., 1998, MNRAS, 296, 483
Keeton C. R., 2001, preprint (astro-ph/0102340)
Keeton C. R., 2003, ApJ, 584, 664
Keeton C. R., Kochanek C. S., Falco E. E., 1998, ApJ, 509, 561
Klypin A., Kravtsov A. V., Valenzuela O., Prada F., 1999, ApJ, 522, 82
Koopmans L. V. E. et al., 2003, ApJ, 595, 712
Kormann R., Schneider P., Bartelmann M., 1994, A&A, 284, 285
Macciò A. V., Miranda M., 2006, MNRAS, 368, 599
Macciò A. V., Moore B., Stadel J., Diemand J., 2006, MNRAS, 366, 1529
Mao S., Schneider P., 1998, MNRAS, 295, 587
Metcalf R. B., 2005a, ApJ, 622, 72
Metcalf R. B., 2005b, ApJ, 629, 673
Metcalf R. B., Madau P., 2001, ApJ, 563, 9
Metcalf R. B., Zhao H., 2002, ApJ, 567, L5
Moore B., Ghigna S., Governato F., Lake G., Quinn T., Stadel J., Tozzi P., 1999, ApJ, 524, L19
Navarro J. F., Frenk C. S., White S. D. M., 1996, ApJ, 462, 563
Patnaik A. R., Narasimha D., 2001, MNRAS, 326, 1403
Peebles P. J. E., 2001, ApJ, 557, 495
Raychaudhury S., Saha P., Williams L. L. R., 2003, AJ, 126, 29
Réfrégier A. et al., 2006, SPIE, 6265, 58
Saha P., Williams L. L. R., Ferreras I., 2007, ApJ, 663, 29
Schechter P. L., Wambsganss J., 2002, ApJ, 580, 685
Schneider P., Weiss A., 1992, A&A, 260, 1
Schneider P., Ehlers J., Falco E. E., 1992, Gravitational Lenses. Springer-Verlag (SEF), Berlin
Sheth R. K., Tormen G., 2002, MNRAS, 329, 61
Seljak U., Zaldarriaga M., 1996, ApJ, 469, 437
Seljak U., Makarov A., McDonald P., Trac H., 2006, Phys. Rev. Lett., 97, 191303
Sluse D. et al., 2003, A&A, 406, L43
Spergel D. N. et al., 2003, ApJ, 148, 175
Spergel D. N. et al., 2007, ApJS, 170, 377
Tonry J. L., 1998, AJ, 115, 1
Treu T., Koopmans L. V. E., 2002, ApJ, 575, 87
Viel M., Lesgourgues J., Haehnelt M. G., Matarrese S., Riotto A., 2005, Phys Rev. D., 71, 063534
Viel M., Lesgourgues J., Haehnelt M. G., Matarrese S., Riotto A., 2006, Phys. Rev. Lett., 97, 071301
Zakharov A. F., 1995, A&A, 293, 1

This paper has been typeset from a TEX/LATEX file prepared by the author.